Editors' Suggestion | Featured in Physics

Bond-Level Imaging of the 3D Conformation of Adsorbed Organic Molecules Using Atomic Force Microscopy with Simultaneous Tunneling Feedback

Daniel Martin-Jimenez,[1,4] Sebastian Ahles,[2,4] Doreen Mollenhauer,[3,4]
Hermann A. Wegner,[2,4] Andre Schirmeisen,[1,4] and Daniel Ebeling[1,4,*]

[1]*Institute of Applied Physics (IAP), Justus Liebig University Giessen, Heinrich-Buff-Ring 16, 35392 Giessen, Germany*
[2]*Institute of Organic Chemistry, Justus Liebig University Giessen, Heinrich-Buff-Ring 17, 35392 Giessen, Germany*
[3]*Institute of Physical Chemistry, Justus Liebig University Giessen, Heinrich-Buff-Ring 17, 35392 Giessen, Germany*
[4]*Center for Materials Research (LaMa), Justus Liebig University Giessen, Heinrich-Buff-Ring 16, 35392 Giessen, Germany*

(Received 13 February 2019; published 13 May 2019)

The chemical structure and orientation of molecules on surfaces can be visualized using low temperature atomic force microscopy with CO-functionalized tips. Conventionally, this is done in constant-height mode by measuring the frequency shift of the oscillating force sensor. However, this method is unsuitable for analyzing 3D objects. We are using the tunneling current to track the topography while simultaneously obtaining submolecular resolution from the frequency shift signal. Thereby, the conformation of 3D molecules and the adsorption sites on the atomic lattice can be reliably determined.

DOI: 10.1103/PhysRevLett.122.196101

The so-called bond imaging technique, which involves the functionalization of the tip of an atomic force microscope (AFM) with a single CO molecule, has become an invaluable tool for studying adsorbed molecules on surfaces [1]. With this method, it became, for instance, possible to identify molecular structures including bond orders, determine adsorption geometries, follow on-surface chemical reactions, and to determine the absolute configuration of chiral compounds [2–24]. In comparison to conventional scanning tunneling microscopy (STM) with unfunctionalized tips, the AFM bond imaging technique offers higher lateral resolution that allows us to gain more detailed and more precise information of the adsorbed molecular species. Apart from this, the STM and AFM image contrasts are generated by different mechanisms, i.e., while in AFM the structure of the molecule mainly determines the image contrast (via interaction forces between the CO tip and imaged molecule), in STM the density of electronic states is the decisive component. Hence, the two different methods offer complementary types of information that are useful for getting a more detailed picture of the studied molecular systems.

In the original application of the bond imaging technique, the CO tip is scanned in constant-height mode (deactivated tip-sample distance feedback) above the sample surface, while the frequency shift (Δf) of the oscillating tuning fork sensor is detected [see Fig. 1(a)]. Repulsive interactions between the CO tip and the atoms of the imaged molecule result in positive frequency shifts (bright image contrast) and attractive interactions lead to negative frequency shifts (dark contrast). Therewith, the internal chemical structure of adsorbed molecules can be made visible, since atoms and the internal bonding structure of molecules appear as bright features in such images.

This method is perfectly suited for the analysis of molecules that adsorb planar on the substrate, such as simple aromatic compounds. However, it is inadequate for studying bulky molecules or adsorption structures that are

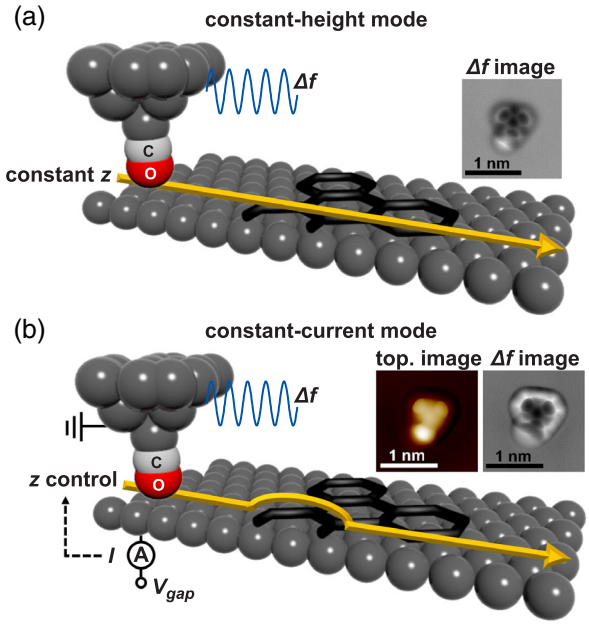

FIG. 1. (a) Scheme of the conventional bond imaging technique. A CO-functionalized tip that is attached to an oscillating tuning fork sensor is scanned in constant-height mode above the surface. The frequency shift signal reveals the chemical structure of the imaged molecule. (b) Scheme of the proposed constant-current mode, where the tunneling current is used to track the sample topography while the frequency shift signal is simultaneously captured for providing submolecular contrast.

slightly deformed, e.g., due to functional groups that are attached to the aromatic system. In a constant-height scan, different regions of such 3D adsorption structures generate different image contrasts since these are located further away or closer to the CO tip, which leads to stronger or weaker interactions. Therefore, images of bulky molecular structures are difficult to interpret. To date, true 3D systems are only scarcely studied, since this involves laborious scanning of different parts of the molecule separately or the application of custom height profiles [7,13,14,17,25].

To circumvent this problem a method involving a tip-sample distance feedback can be utilized. Usually, the frequency shift signal is used for this purpose [26]. Unfortunately, the frequency shift due to the interactions between the CO tip and the atoms of the adsorbed molecule is rather low (on the order of a few Hz). Therefore, a frequency shift-based tip-sample feedback would require very long data acquisition times (note that the typical measurement bandwidth of the frequency shift detection for achieving submolecular resolution is around 10 Hz, which would require unreasonable data acquisition times on the order of several 100 ms/pixel).

Promising approaches for directly imaging 3D adsorption structures are, e.g., so-called "two-pass" methods where the topography of the sample is recorded in a first pass (with parameters optimized for tip-sample distance feedback and without submolecular resolution), while the second pass follows the predetermined height profile with deactivated feedback and parameters optimized for achieving high resolution [27,28]. Recently, we proposed the use of modern multifrequency techniques such as bimodal AFM to simultaneously track the topography of the sample and achieve submolecular resolution using CO-functionalized tips [29]. Bimodal AFM [30,31] can be applied to utilize two oscillation eigenmodes of the tuning fork sensor simultaneously, one for the tip-sample feedback and another one to achieve submolecular resolution [32–34]. However, this requires additional electronics, which are usually not available with standard setups.

Here, we are proposing an even simpler method where the STM signal is used for tip-sample distance feedback by keeping the tunneling current (I) at a constant value during imaging single adsorbed molecules with a CO-functionalized tip [Fig. 1(b)]. Simultaneously, the frequency shift signal of the tuning fork sensor is recorded for achieving submolecular contrast (as done in the conventional constant-height mode). In the case of small adsorbed iron clusters on a Cu(111) surface this method has been successfully applied to determine their adsorption sites [35].

We present a systematic study of the constant-current method for imaging single organic molecules and compare the obtained image contrast with the conventional constant-height scanning. We are revealing the similarities and differences of the two methods and demonstrate that the additional information that is obtained when scanning with

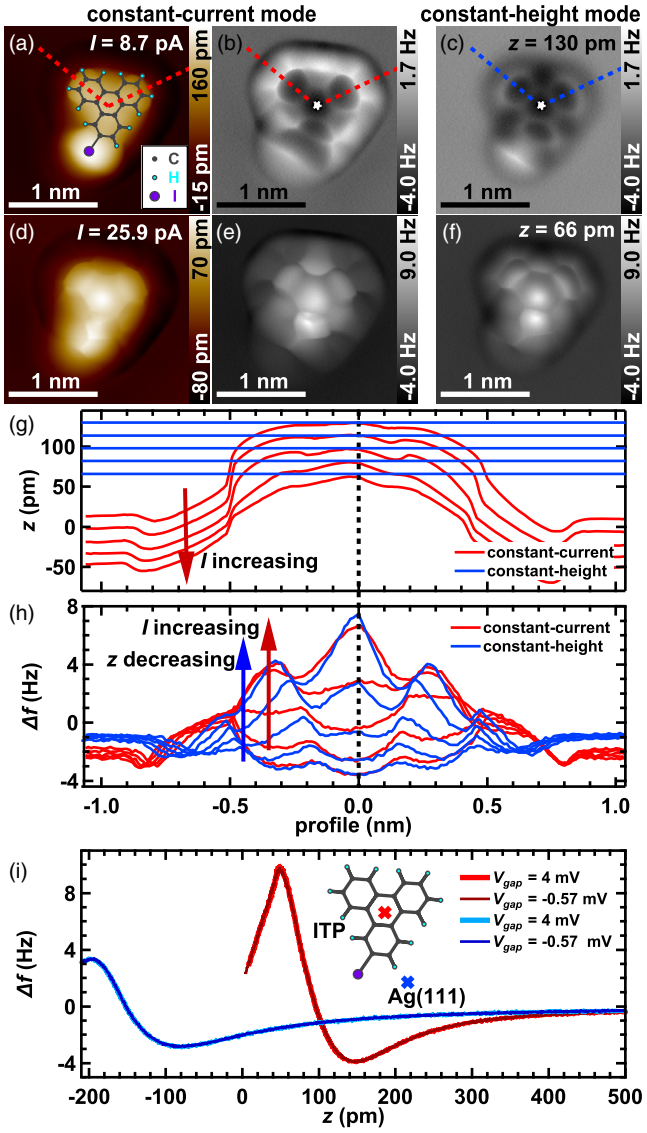

FIG. 2. (a),(d) Topography and (b),(e) frequency shift images of ITP in constant-current mode for two tunneling currents ($I = 8.7$ and 25.9 pA, $V_{gap} = 4$ mV, oscillation amplitude = 52 pm). (c), (f) Constant-height frequency shift images for two imaging distances ($z = 130$ and 66 pm). (g),(h) Topography and frequency shift profiles along red and blue dashed lines in Fig. 2(a)–2(c) for $I = 8.7$, 11.6, 15.5, 20.4, and 25.9 pA (constant-current mode) and $z = 130$, 114, 98, 82, and 66 pm (constant-height mode). Red and blue arrows indicate increasing currents (I) and decreasing distances (z), respectively. (i) $\Delta f(z)$ curves on ITP (red color) and Ag(111) (blue color) for $V_{gap} = 4$ and -0.57 mV, respectively.

activated STM feedback can be useful for identifying molecular adsorption structures and the corresponding adsorption sites.

Figure 2 shows images of 2-iodotriphenylene (ITP) ($C_{18}H_{11}I$) [see structure in Figs. 2(a) and 3(a)] on a Ag(111) surface that were obtained with a CO-functionalized tip at a temperature of approx. 5 K and a scanning

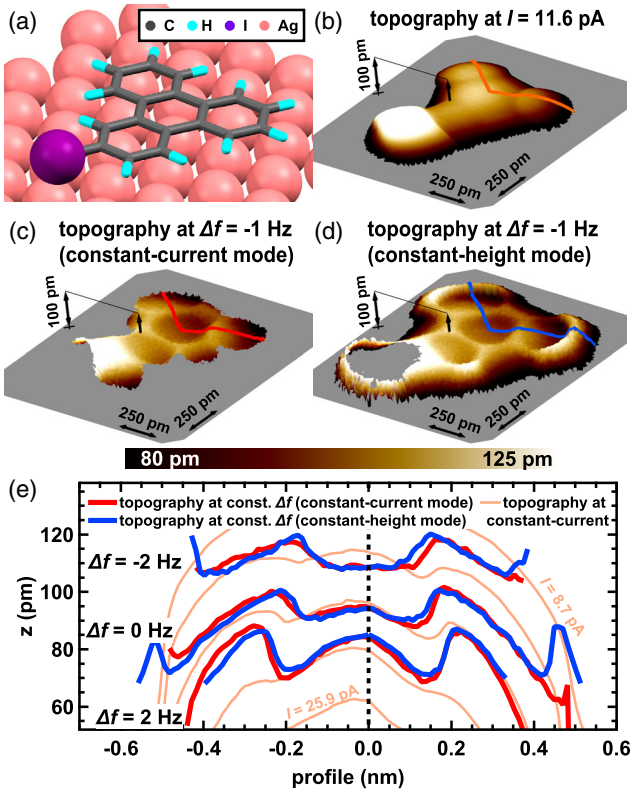

FIG. 3. (a) Sketch of ITP on Ag(111). (b) Topography image of ITP at $I = 11.6$ pA and $V_{\mathrm{gap}} = 4$ mV (oscillation amplitude = 52 pm). (c),(d) Topography images at constant $\Delta f = -1$ Hz for constant-current and constant-height scanning modes. Image pixels that lie outside the proper frequency range for calculating the topography are transparent. The gray planes are set at $z = 66$ pm. (e) Topography profiles at three constant Δf values (-2, 0, 2 Hz) along the red and blue lines in Figs. 3(c),3(d) and topography profiles at constant current ($I = 8.7$, 11.6, 15.5, 20.4, and 25.9 pA) along the orange line in Fig. 3(b).

speed of 625 pm/s (as all other images in this Letter, please see the Supplemental Material for additional experimental details [36]). The constant-current mode images [showing the topography in Figs. 2(a) and 2(d), and the frequency shift in Figs. 2(b) and 2(e)] are directly compared to conventional constant-height frequency shift images [Figs. 2(c) and 2(f)]. To get a detailed picture of the contrast formation process the measurements have been performed for a series of nine different STM setpoints and AFM imaging distances, respectively. The used STM setpoints and AFM imaging distances have been determined carefully from spectroscopy curves [$I(z)$ and $\Delta f(z)$] in order to guarantee similar imaging conditions (the full data set is shown in the Supplemental Material [36]).

The first and second rows in Fig. 2 depict the first and last frames of the image series, respectively. Apparently, the frequency shift images that are obtained in the two different operation modes at comparable tip-sample distances [cf. Figs. 2(b) and 2(e) vs 2(c) and 2(f)] reveal both similarities and differences as will be discussed next. In particular, the image contrast around the central carbon ring [see white dot in Figs. 2(b) and 2(c)] is in remarkable agreement. This can be inferred from the single frequency shift scanlines that are depicted in Fig. 2(h). In the central region the absolute frequency shift values are in good agreement and also the positions of minima and maxima in the curves coincide with each other. Therefore, the apparent size of the central carbon ring is similar for the two operation modes. $\Delta f(z)$ spectroscopy curves that have been taken above the molecule and Ag(111) with and without an applied gap voltage reveal that the Δf signal is rather independent of the tunneling current [Fig. 2(i)]. This explains the good agreement of absolute Δf values.

However, at the edge region of the molecule the images look significantly different [cf. Figs. 2(b) and 2(c)]. This is caused by the STM feedback that moves the tip closer to the Ag(111) surface when the CO tip is not scanning directly above the molecule. This can be inferred from the single topography scanlines that are depicted in Fig. 2(g). Above the center of the molecule (see dashed black lines) the constant-current topography scan lines (red) coincide with the blue lines that correspond to the chosen z values of the constant-height scans. At the edges of the molecule, however, the red lines lie below the blue lines, resulting in stronger interactions between the edge atoms of the molecule and the CO tip in constant-current mode. This behavior is also reflected by the frequency shift scanlines presented in Fig. 2(h). While around the center of the molecule the frequency shift of the two operation modes is very similar, at the edges of the molecule higher absolute values are observed for the constant-current mode.

Next, we compare the quantitative topographical information that can be obtained in the two different operation modes. Therefore, we used the series of frequency shift images at different imaging distances and current setpoints and converted them into topography images by extracting the z values at constant frequency shifts (see Supplemental Material [36] for technical details). This is similar to standard frequency modulation AFM imaging, where the feedback electronics adjusts the tip-sample distance in order to maintain a constant frequency shift setpoint [26]. Therewith, we are able to decouple the electronic and structural topographical information that is simultaneously obtained in constant-current mode.

An example is shown in Figs. 3(b)–3(d) for the ITP molecule on Ag(111). The topography at constant $I = 11.6$ pA and constant $\Delta f = -1$ Hz in constant-current scanning mode are depicted in Figs. 3(b) and 3(c), respectively. The corresponding topography at $\Delta f = -1$ Hz in constant-height mode is shown in Fig. 3(d). Around the central parts of the molecule the topography images 3(c) and 3(d) are in good quantitative agreement, which demonstrates the validity of the decoupling of electronic and structural information in constant-current mode. This is supported by the single topographical

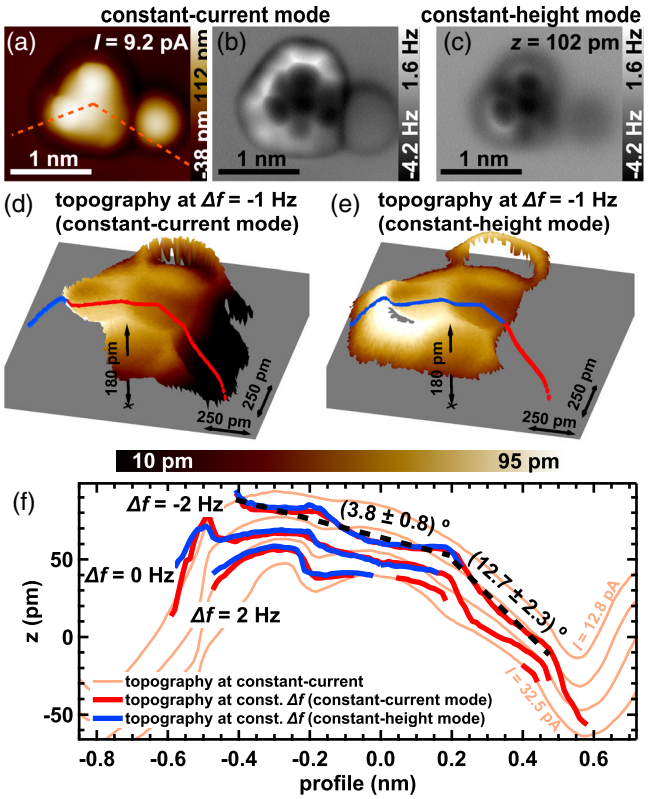

FIG. 4. (a) Topography and (b),(c) frequency shift images of TP radical in constant-current mode ($I = 9.2$ pA, $V_{\mathrm{gap}} = 4$ mV, oscillation amplitude $= 52$ pm) and constant-height mode ($z = 102$ pm), respectively. (d),(e) Topography images of TP radical at constant $\Delta f = -1$ Hz for constant-current and constant-height scanning modes. The gray planes are set at $z = -60$ pm. (f) Topography profiles at three constant Δf values (-2, 0, 2 Hz) along the lines in Figs. 4(d),4(e) and topography profiles at constant current ($I = 12.8$, 17.8, 24.3, and 32.5 pA) along the orange line in Fig. 4(a). The black dashed lines represent linear fits to the topography profiles for determining the tilt of the different regions of the molecule.

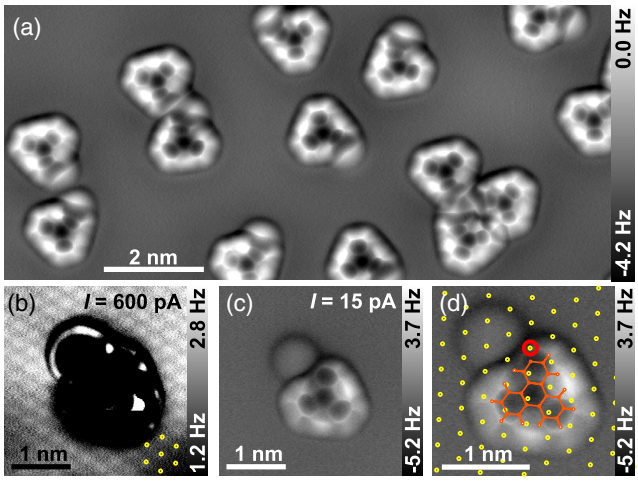

FIG. 5. (a) Frequency shift image of single and self-assembled ITP molecules on Ag(111) in constant-current mode ($I = 25$ pA, $V_{\mathrm{gap}} = 7$ mV and oscillation amplitude $= 68$ pm). (b),(c) Frequency shift images of TP radical on Ag(111) in constant-current mode [$I = 600$ pA in (b) for imaging Ag(111) surface atoms, $I = 15$ pA in (c) for submolecular resolution on ITP molecule]. Other parameters: $V_{\mathrm{gap}} = 2$ mV, oscillation amplitude $= 43$ pm. (d) Overlay of fitted Ag(111) lattice (yellow circles) and molecular structure of TP (orange). The adsorption site is indicated by a red circle.

scanlines presented in Fig. 3(e), which are in good quantitative agreement over a wide range of frequency shift values (-2 to $+2$ Hz). Please note that in Fig. 3(c) no topography values can be determined at the edges off the molecule, which is caused by the chosen range of current setpoints that are optimized for obtaining precise topographical data around the central part of the molecule.

The real strength of the constant-current method certainly comes into play when analyzing 3D adsorption geometries of molecules. To this end, we chose a dehalogenated ITP molecule (adsorbed TP radical) as a test object, since this assumes a complex 3D adsorption structure that is difficult to interpret using the conventional constant-height technique [13,23]. The dehalogenation reaction was locally triggered using a voltage pulse (see Supplemental Material for details [36]). Images of the adsorbed radical and the cleaved iodine atom taken in the two different operation modes are depicted in Figs. 4(a)–4(c). It is clearly revealed that the deiodinated aryl ring bends with its radical position towards the Ag(111) surface. In constant-height mode only a very small part of this aryl ring is visible due to its larger distance to the CO tip. By contrast, in constant-current mode large parts of this bent aryl ring are still imaged due to the activated tip-sample feedback.

A series of nine different scans at different imaging distances and tunneling setpoints was measured (see Fig. S2 [36]) and corresponding topography images at constant Δf were determined [see Figs. 4(d) and 4(e)]. These images reveal that the constant-current mode is capable of imaging a larger portion of the heavily tilted adsorption structure. Single topography scanlines are presented in Fig. 4(f), which allow to directly fit the adsorption angles of the molecule with respect to the Ag(111) plane (see dashed black lines). Whereas the pristine molecule adsorbed almost parallel to the Ag(111) surface [Fig. 3(e)], the adsorbed radical is slightly tilted and, in particular, the deiodinated aryl ring is significantly bent towards the surface [cf. Fig. 4(f)]. For the part of the molecule which is relatively flat we observe a tilting angle of $3.8° \pm 0.8°$ in both operation modes. The aryl ring with the radical site is tilted by $12.7° \pm 2.3°$. The latter information is only obtained in constant-current mode, since this aryl ring is not detected in constant-height mode. Besides the molecules analyzed here, we have used the proposed method for studying aliphatic compounds such as bulky [121]tetramantane; see Ref. [14], which demonstrates the versatility of the method.

Finally, we emphasize two other useful areas of application for the proposed constant-current mode. First, the

constant-current mode is ideally suited for safely performing large overview scans with submolecular resolution [see Fig. 5(a)]. This is beneficial for obtaining statistical information about the orientation of molecules on different terraces or if any other 3D obstacles impede constant-height scanning [22]. Second, the method is very useful for a precise determination of the specific adsorption sites of a molecule. Figures 5(b) and 5(c) show two subsequent constant-current scans of an adsorbed TP radical that have been optimized for obtaining atomic resolution of the Ag(111) surface and on the molecule, respectively. This allows us to overlay the fitted Ag(111) lattice (yellow circles) with the structure of the molecule [Fig. 5(d)]. Therewith, the Ag(111) surface atom, which binds to the radical position of the deiodinated aryl ring [see red circle in Fig. 5(d)] can be unambiguously assigned.

To obtain such information using the constant-height technique, the substrate in the close vicinity of the molecule has to be scanned separately and the fitted atomic lattice has to be extrapolated over the region where the molecule is adsorbed [49]. On one hand this latter method offers a lower risk of a tip change since the CO tip does not need to be approached extremely close to the molecule in order to achieve atomic contrast on the substrate. On the other hand, the constant-current method is intrinsically more precise since no extrapolation of the lattice is needed.

Our results demonstrate that the chemical structure of single adsorbed molecules can be revealed by constant-current AFM with CO-functionalized tips. The measured signals in the constant-current mode contain structural and electronic components that can be reliably decoupled. Hence, for flat molecules that adsorb planar to the surface the structural topographical information of the constant-current and constant-height scanning modes are in good quantitative agreement. In particular, for identifying adsorption structures of 3D molecular objects the constant-current technique is beneficial due to the activated tip-sample feedback. In addition, the constant-current mode offers advantages for the precise identification of adsorption sites and for large overview scans. Therewith, the proposed methodology represents a valuable addition to the well-established constant-height bond imaging technique that is useful for obtaining more detailed and more precise information about the 3D conformation of adsorbed molecules.

Financial support by the Deutsche Forschungsgemeinschaft (DFG) via Grant No. EB 535/1-1 and via the GRK (Research Training Group) 2204 "Substitute Materials for Sustainable Energy Technologies" is gratefully acknowledged.

*Corresponding author.
daniel.ebeling@ap.physik.uni-giessen.de

[1] L. Gross, F. Mohn, N. Moll, P. Liljeroth, and G. Meyer, Science **325**, 1110 (2009).
[2] L. Gross, F. Mohn, N. Moll, G. Meyer, R. Ebel, W. M. Abdel-Mageed, and M. Jaspars, Nat. Chem. **2**, 821 (2010).
[3] L. Gross, F. Mohn, N. Moll, B. Schuler, A. Criado, E. Guitián, D. Peña, A. Gourdon, and G. Meyer, Science **337**, 1326 (2012).
[4] D. G. de Oteyza *et al.*, Science **340**, 1434 (2013).
[5] J. Zhang, P. Chen, B. Yuan, W. Ji, Z. Cheng, and X. Qiu, Science **342**, 611 (2013).
[6] J. Van Der Lit, M. P. Boneschanscher, D. Vanmaekelbergh, M. Ijäs, A. Uppstu, M. Ervasti, A. Harju, P. Liljeroth, and I. Swart, Nat. Commun. **4**, 2023 (2013).
[7] F. Albrecht, N. Pavliček, C. Herranz-Lancho, M. Ruben, and J. Repp, J. Am. Chem. Soc. **137**, 7424 (2015).
[8] M. Ellner, N. Pavliček, P. Pou, B. Schuler, N. Moll, G. Meyer, L. Gross, and R. Pérez, Nano Lett. **16**, 1974 (2016).
[9] P. Ruffieux *et al.*, Nature (London) **531**, 489 (2016).
[10] A. Riss *et al.*, Nat. Chem. **8**, 678 (2016).
[11] O. Stetsovych, M. Švec, J. Vacek, J. V. Chocholoušová, A. Jančařík, J. Rybáček, K. Kosmider, I. G. Stará, and P. Jelínek Nat. Chem. **9**, 213 (2017).
[12] P. H. Jacobse, A. Kimouche, T. Gebraad, M. M. Ervasti, M. Thijssen, P. Liljeroth, and I. Swart, Nat. Commun. **8**, 119 (2017).
[13] S. Zint, D. Ebeling, T. Schlöder, S. Ahles, D. Mollenhauer, H. A. Wegner, and A. Schirmeisen, ACS Nano **11**, 4183 (2017).
[14] D. Ebeling, M. Šekutor, M. Stiefermann, J. Tschakert, J. E. P. Dahl, R. M. K. Carlson, A. Schirmeisen, and P. R. Schreiner, ACS Nano **11**, 9459 (2017).
[15] S. Kawai, T. Nishiuchi, T. Kodama, P. Spijker, R. Pawlak, T. Meier, J. Tracey, T. Kubo, E. Meyer, and A. S. Foster, Sci. Adv. **3**, e1603258 (2017).
[16] R. Pawlak *et al.*, ACS Nano **11**, 9930 (2017).
[17] D. Ebeling, M. Šekutor, M. Stiefermann, J. Tschakert, J. E. P. Dahl, R. M. K. Carlson, A. Schirmeisen, and P. R. Schreiner, Nat. Commun. **9**, 2420 (2018).
[18] Q. Fan, S. Werner, J. Tschakert, D. Ebeling, A. Schirmeisen, G. Hilt, W. Hieringer, and J. M. Gottfried, J. Am. Chem. Soc. **140**, 7526 (2018).
[19] X. L. Su, Z. J. Xue, G. Li, and P. Yu, Nano Lett. **18**, 5744 (2018).
[20] C.-H. Shu, M.-X. Liu, Z.-Q. Zha, J.-L. Pan, S.-Z. Zhang, Y.-L. Xie, J.-L. Chen, D.-W. Yuan, X.-H. Qiu, and P.-N. Liu, Nat. Commun. **9**, 2322 (2018).
[21] H. Mönig *et al.*, Nat. Nanotechnol. **13**, 371 (2018).
[22] Q. Zhong, D. Ebeling, J. Tschakert, Y. Gao, D. Bao, S. Du, C. Li, L. Chi, and A. Schirmeisen, Nat. Commun. **9**, 3277 (2018).
[23] D. Ebeling, Q. Zhong, T. Schlöder, J. Tschakert, P. Henkel, S. Ahles, L. Chi, D. Mollenhauer, H. A. Wegner, and A. Schirmeisen, ACS Nano **13**, 324 (2019).
[24] M. Ellner, P. Pou, and R. Pérez, ACS Nano **13**, 786 (2019).
[25] N. Pavliček, B. Schuler, S. Collazos, N. Moll, D. Pérez, E. Guitián, G. Meyer, D. Peña, and L. Gross, Nat. Chem. **7**, 623 (2015).
[26] T. R. Albrecht, P. Grütter, D. Horne, and D. Rugar, J. Appl. Phys. **69**, 668 (1991).
[27] C. Moreno, O. Stetsovych, T. K. Shimizu, and O. Custance, Nano Lett. **15**, 2257 (2015).

[28] M. P. Boneschanscher, J. Van Der Lit, Z. Sun, I. Swart, P. Liljeroth, and D. Vanmaekelbergh, ACS Nano **6**, 10216 (2012).
[29] D. Ebeling, Q. G. Zhong, S. Ahles, L. Chi, H. A. Wegner, and A. Schirmeisen, Appl. Phys. Lett. **110**, 183102 (2017).
[30] T. R. Rodriguez and R. Garcia, Appl. Phys. Lett. **84**, 449 (2004).
[31] R. Garcia and E. T. Herruzo, Nat. Nanotechnol. **7**, 217 (2012).
[32] D. Ebeling, B. Eslami, and S. D. Solares, ACS Nano **7**, 10387 (2013).
[33] D. Ebeling and S. D. Solares, Nanotechnology **24**, 135702 (2013).
[34] D. Ebeling and S. D. Solares, Beilstein J. Nanotechnol. **4**, 198 (2013).
[35] M. Emmrich *et al.*, Science **348**, 308 (2015).
[36] See Supplemental Material at http://link.aps.org/supplemental/10.1103/PhysRevLett.122.196101 for further details, which includes Refs. [37–48].
[37] R. Nandy and S. Sankararaman, Org. Biomol. Chem. **8**, 2260 (2010).
[38] G. H. Simon, M. Heyde, and H.-P. Rust, Nanotechnology **18**, 255503 (2007).
[39] TURBOMOLE V6.6 2014, a development of University of Karlsruhe and Forschungszentrum Karlsruhe GmbH, 1989-2007, TURBOMOLE GmbH, since 2007; available from http://www.turbomole.com.
[40] A. D. Becke, Phys. Rev. A **38**, 3098 (1988).
[41] J. P. Perdew and W. Yue, Phys. Rev. B **33**, 8800 (1986).
[42] S. Grimme, J. Antony, S. Ehrlich, and H. Krieg, J. Chem. Phys. **132**, 154104 (2010).
[43] O. Treutler and R. Ahlrichs, J. Chem. Phys. **102**, 346 (1995).
[44] M. Von Arnim and R. Ahlrichs, J. Comput. Chem. **19**, 1746 (1998).
[45] K. Eichkorn, O. Treutler, H. Oehm, M. Haeser, and R. Ahlrichs, Chem. Phys. Lett. **242**, 652 (1995).
[46] K. Eichkorn, F. Weigend, O. Treutler, and R. Ahlrichs, Theor. Chem. Acc. **97**, 119 (1997).
[47] T. H. Dunning, Jr., J. Chem. Phys. **90**, 1007 (1989).
[48] K. A. Peterson, B. C. Shepler, D. Figgen, and H. Stoll, J. Phys. Chem. A **110**, 13877 (2006).
[49] B. Schuler, W. Liu, A. Tkatchenko, N. Moll, G. Meyer, A. Mistry, D. Fox, and L. Gross, Phys. Rev. Lett. **111**, 106103 (2013).